

# Ghost imaging protocol with intense correlated fields for efficient encryption

E. Puddu<sup>1,\*</sup>, I. P. Degiovanni<sup>2,†</sup>, A. Andreoni<sup>1</sup>, M. Bondani<sup>3</sup>, and S. Castelletto<sup>4</sup>

<sup>1</sup>*Dipartimento di Fisica e Matematica,  
Università degli Studi dell'Insubria and Consiglio Nazionale delle Ricerche,  
Istituto Nazionale per la Fisica della Materia (C.N.R.-I.N.F.M.),  
Via Valleggio, 11 - 22100 Como, Italy*

<sup>2</sup>*Istituto Nazionale di Ricerca Metrologica,  
Strada delle Cacce 91 - 10135 Torino (Italy)*

<sup>3</sup>*National Laboratory for Ultrafast and Ultraintense Optical Science - C.N.R.-I.N.F.M.,  
Via Valleggio, 11 - 22100 Como, Italy*

<sup>4</sup>*Physics School, Melbourne University, Victoria, Australia*

(Dated: February 9, 2020)

We present a proof of principle of a straightforward application of distributed imaging to the efficient encryption of images. The basic idea is to exploit, in a ghost-imaging experiment, the correlations of the fields produced by a chaotically seeded parametric downconversion to deduce a Code for reconstructing the image of the object. As we demonstrate that this Code is smaller than the entire image size, we suggest that this technique can be used for more efficient image encryption by any quantum key.

PACS numbers: 42.50.-p, 42.65.Lm, 03.67.Dd, 03.67.Hk

Quantum key distribution (QKD) is a direct application of fundamental quantum mechanics, involving two parties, Alice and Bob, exchanging some classical information. By QKD Alice and Bob share secret random keys to implement a secure encryption-decryption algorithm (one-time-pad) without meeting, and the security of the distributed keys is based on the laws of quantum physics [1]. However at variance with classical communication that can be performed at a rate of Gbyte/s, though in an insecure way, practical QKD protocols, in their up-to-date best realizations, allow secure quantum key rates below 10 Kbit/s, possibly improved to 100 Kbit/s in the next ten years [2]. Therefore, as the length of the key must necessarily equal the length of the message to guarantee absolute security, for a real world application quantum keys can be used only for encrypting the most sensitive parts of the messages. In protocols for secure image transmission [3, 4, 5], the problem cannot be easily bypassed because any image must be encrypted as a whole.

Here we propose a proof of principle experiment which may help solving the problem that the usual size of an image requires a long secure quantum key by using the properties of a ghost imaging protocol with intense correlated fields. In particular, our implementation of the ghost imaging protocol follows consolidated procedures as to detection and data manipulation [6], but it is original as to the light source. In fact we used the correlated beams generated by parametric downconversion (PDC) seeded with chaotic light.

The measurements performed at Alice's laboratory are the following ones (see Fig. 1): the beam containing the

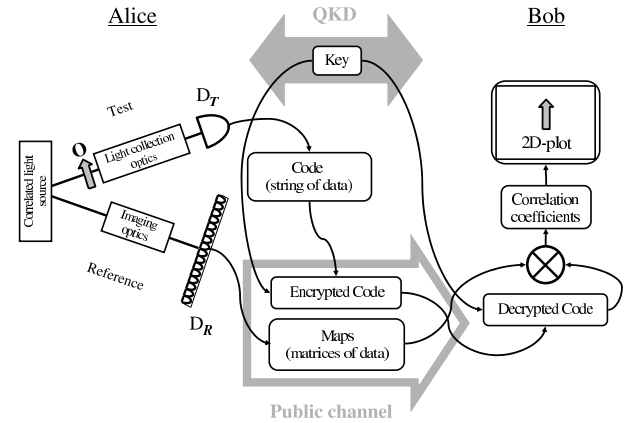


FIG. 1: Scheme of an efficient encryption of the image of an object by distributed imaging.

object (Test-arm beam) is measured with a bucket detector,  $D_T$ , which does not provide any information on the spatial intensity distribution, while the other beam (Reference-arm beam) is measured by a position sensitive detector, namely a CCD camera,  $D_R$ . Neither of the two sets of data separately carries information that is suitable to reconstruct the image of the object, but they represent a pair of complementary sets from which Bob will univocally determine the object shape. The basic idea is that one of the sets can serve as the Code to convert the information carried by the other set into the image of the real object. As the Code, we adopt the data set recorded by  $D_T$ , which is a string of numbers, whereas the set of Maps recorded by  $D_R$  is a collection of two-dimensional matrices of data. As shown in Fig. 1, Alice and Bob exchange a quantum cryptographic Key by using a QKD protocol (*e.g.* BB84 or B92) [1]. Alice owns the object of which she wants to securely transmit the image to Bob.

\*Electronic address: emiliano.puddu@uninsubria.it

†Electronic address: degio@ien.it

She records  $N$  chaotic Maps and the corresponding  $N$  values that constitute the Code. In our scheme only the Code undergoes the one-time-pad protocol [1], instead of the whole image. Via a public non-jammable channel [1], Alice sends Bob the sequence of the Maps and the Code encrypted by the Key. Bob decrypts the Code, performs the calculation of the fourth-order correlation coefficients between the Maps and the Code and obtains 2D-plots that display the recovered image.

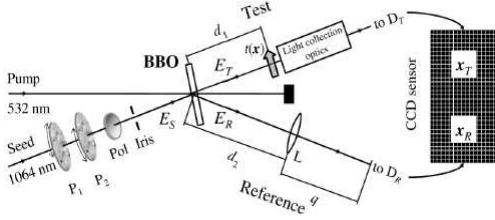


FIG. 2: Experimental setup:  $P_{1,2}$ , independently rotating ground glass plates; Pol, polarizer;  $t(\mathbf{x})$ , object transmission function; L, lens. The CCD sensor is used to detect both Test and Reference beams.

In Fig. 2 we show our experimental setup. We injected

a coherent collimated pump beam ( $\lambda = 532$  nm) and a seed beam ( $\lambda = 1064$  nm) into a crystal of  $\beta$ -BaB<sub>2</sub>O<sub>4</sub> (BBO, cut angle 22.8 deg, 10 mm×10 mm×3 mm, Fujian Castech Crystals, China). Both pump and seed beams were provided by an amplified Q-switched Nd:YAG laser (GCR-4, 10 Hz repetition rate, 7 ns pulse duration of the fundamental pulse, Spectra-Physics, USA). The seed field was randomized by passing it through two independently rotating ground glass plates,  $P_1$  and  $P_2$  in order to obtain a pseudo-thermal statistics. The speckle size on the object plane resulted to be about 320  $\mu\text{m}$  in diameter. We describe the interaction in the crystal by using the input-output relations [7]

$$b_i(\mathbf{q}) = U_i(\mathbf{q})a_i(\mathbf{q}) + V_i(\mathbf{q})a_j^\dagger(-\mathbf{q}) \quad i = R, T; i \neq j. \quad (1)$$

that link the output operators  $b_i(\mathbf{q})$  with the input operators  $a_i(\mathbf{q})$  ( $|U_i(\mathbf{q})|^2 - |V_i(\mathbf{q})|^2 = 1$ ). At the crystal input, the field in the Reference arm is in the vacuum state and that in the Test arm in a multimode thermal state:

$$\rho_T = \prod_{\mathbf{q}} \left\{ \sum_{m=0}^{\infty} p_T[m(\mathbf{q})] |m(\mathbf{q})\rangle_{TT} \langle m(\mathbf{q})| \right\} \quad (2)$$

where  $|m(\mathbf{q})\rangle$  denotes the Fock state with  $m$  photons in mode  $\mathbf{q}$  and  $p_T[m] = [n_{th}(\mathbf{q})]^m / [1 + n_{th}(\mathbf{q})]^{m+1}$  is the photon number distribution on the single mode for  $n_{th}(\mathbf{q})$  mean photon number. In the degenerate case and neglecting losses we can assume  $V_R(\mathbf{q}) = V_T(\mathbf{q})$ . The density matrix at the output is then [8]

$$\rho_{out} = \prod_{\mathbf{q}} \sum_{n(\mathbf{q})} p_T[n(\mathbf{q})] \sum_{n_1(\mathbf{q}), n_2(\mathbf{q})} F[n(\mathbf{q}), n_1(\mathbf{q}), n_2(\mathbf{q})] |n(\mathbf{q}) + n_1(\mathbf{q})\rangle_{TT} \langle n(\mathbf{q}) + n_2(\mathbf{q})| \otimes |n_1(-\mathbf{q})\rangle_{RR} \langle n_2(-\mathbf{q})| \quad (3)$$

where we have defined

$$F[n(\mathbf{q}), n_1(\mathbf{q}), n_2(\mathbf{q})] = \frac{[n_{\text{PDC}}(\mathbf{q})]^{\frac{n_1(\mathbf{q}) + n_2(\mathbf{q})}{2}}}{[1 + n_{\text{PDC}}(\mathbf{q})]^{n(\mathbf{q}) + 1 + \frac{n_1(\mathbf{q}) + n_2(\mathbf{q})}{2}}} \times \sqrt{\frac{[n(\mathbf{q}) + n_1(\mathbf{q})]!}{n(\mathbf{q})! n_1(\mathbf{q})!}} \sqrt{\frac{[n(\mathbf{q}) + n_2(\mathbf{q})]!}{n(\mathbf{q})! n_2(\mathbf{q})!}} \quad (4)$$

being  $n_{\text{PDC}}(\mathbf{q}) = |V_R(\mathbf{q})|^2$  the mean photon number per mode generated by the spontaneous PDC process. It can be demonstrated [9] that the inseparable state  $\rho_{out}$  becomes separable as soon as the mean number of seeding thermal photons,  $n_{th}(\mathbf{q})$ , exceeds a threshold, namely

$$n_{th}(\mathbf{q}) > n_{\text{PDC}}(\mathbf{q}) + \sqrt{n_{\text{PDC}}(\mathbf{q}) (n_{\text{PDC}}(\mathbf{q}) + 1)} \quad (5)$$

In our experimental conditions with a pump intensity  $\sim 70$  MW/cm<sup>2</sup>,  $n_{\text{PDC}} \simeq 0.5$ . On the other hand, based

on an evaluation of the speckle number in the seed-beam cross-section and of the energy of the seeding pulse, we estimate  $n_{th} \simeq 10^{12}$  per coherence area (spatial mode). Thus our correlated beams should not be entangled.

The object was a hole of 1.6 mm diameter crossed by a straight wire of 0.5 mm caliber. As the  $D_T$  and  $D_R$  detectors, we used a single CCD camera (CA-D1-256T, 16  $\mu\text{m} \times 16$   $\mu\text{m}$  pixel area, 12 bit resolution, Dalsa, Canada). The CCD sensor, also depicted in Fig. 2, for one half recorded the single-shot intensity Maps in the Reference arm,  $I_R(\mathbf{x}_R)$ , and for the other half realized the bucket detector of the Test arm. In the following,  $I_T$  designates the sum of the contents of the pixels of  $D_T$ . The Test arm includes free propagation over distance  $d_1 = 60$  cm from BBO to object, see transmission  $t(\mathbf{x})$ , and light collection optics in front of the  $D_T$ . The Reference arm contains free propagation from BBO to lens L (focal length

$f = 400$  mm,  $d_2 = 60$  cm) and from L to the CCD camera (distance  $q = 60$  cm). Distances  $d_1$ ,  $d_2$  and  $q$  must satisfy  $1/(d_1 + d_2) + 1/q = 1/f$  [10] to give an imaging system with magnification factor  $M = q/(d_1 + d_2)$ . In our case  $M = 0.5$ .

The reconstruction of the image of the object is achieved by the computation of the correlation function,  $G^{(2)}(\mathbf{x}_R)$ , between the fluctuations of recorded values  $I_T$  of the photon flux on the bucket detector and those of the photon flux on each pixel on the Reference arm  $I_R(\mathbf{x}_R)$ . This procedure is equivalent to evaluating first the correlation function between  $I_R(\mathbf{x}_R)$  and  $I_T(\mathbf{x}_T)$ :

$$G^{(2)}(\mathbf{x}_R, \mathbf{x}_T) = \langle I_R(\mathbf{x}_R)I_T(\mathbf{x}_T) \rangle - \langle I_R(\mathbf{x}_R) \rangle \langle I_T(\mathbf{x}_T) \rangle, \quad (6)$$

and then integrating over all the values of  $\mathbf{x}_T$

$$G^{(2)}(\mathbf{x}_R) = \int d\mathbf{x}_T G^{(2)}(\mathbf{x}_R, \mathbf{x}_T), \quad (7)$$

where  $\langle I_i(\mathbf{x}_i) \rangle = \langle c_i^\dagger(\mathbf{x}_i)c_i(\mathbf{x}_i) \rangle$  ( $i = R, T$ ) is the mean intensity of the  $i$ -th beam and  $\langle I_R(\mathbf{x}_R)I_T(\mathbf{x}_T) \rangle = \langle c_R^\dagger(\mathbf{x}_R)c_R(\mathbf{x}_R)c_T^\dagger(\mathbf{x}_T)c_T(\mathbf{x}_T) \rangle$ . The propagation of the two outgoing beams through the optical paths described above is summarized in two impulse response functions  $h_R(\mathbf{x}_R, \mathbf{x}'_R)$  and  $h_T(\mathbf{x}_T, \mathbf{x}'_T)$ , whose derivation is straightforward [11]. The field operators at the detection planes are thus given by

$$c_i(\mathbf{x}_i) = \int d\mathbf{x}'_i h_i(\mathbf{x}_i, \mathbf{x}'_i) b_i(\mathbf{x}'_i). \quad (8)$$

where  $b_i(\mathbf{x}) = \int d\mathbf{q}/(2\pi) e^{i\mathbf{q}\cdot\mathbf{x}} b_i(\mathbf{q})$  are the Reference and Test field operators at the output face of the crystal. By means of Eq.s (1) we can demonstrate [8] that the factorization rule for  $\langle b_R^\dagger(\mathbf{x}''_R) b_R(\mathbf{x}'_R) b_T^\dagger(\mathbf{x}''_T) b_T(\mathbf{x}'_T) \rangle$  is the same as for spontaneous PDC [7]

$$\begin{aligned} \langle b_R^\dagger(\mathbf{x}''_R) b_R(\mathbf{x}'_R) b_T^\dagger(\mathbf{x}''_T) b_T(\mathbf{x}'_T) \rangle = \\ \langle b_R^\dagger(\mathbf{x}''_R) b_R(\mathbf{x}'_R) \rangle \langle b_T^\dagger(\mathbf{x}''_T) b_T(\mathbf{x}'_T) \rangle \\ + \langle b_R^\dagger(\mathbf{x}''_R) b_T^\dagger(\mathbf{x}''_T) \rangle \langle b_R(\mathbf{x}'_R) b_T(\mathbf{x}'_T) \rangle, \end{aligned} \quad (9)$$

where  $\langle \dots \rangle = \text{Tr}(\dots |0_R\rangle\langle 0_R| \otimes \rho_T)$ . Thus in the degenerate case Eq. (6) becomes

$$\begin{aligned} G^{(2)}(\mathbf{x}_R, \mathbf{x}_T) = \\ \left| \int d\mathbf{x}'_R \int d\mathbf{x}'_T h_R(\mathbf{x}_R, \mathbf{x}'_R) h_T(\mathbf{x}_T, \mathbf{x}'_T) \langle b_R(\mathbf{x}'_R) b_T(\mathbf{x}'_T) \rangle \right|^2 \end{aligned} \quad (10)$$

leading to

$$\begin{aligned} G^{(2)}(\mathbf{x}_R) \propto |t(-M\mathbf{x}_R)|^2 \int d\mathbf{x}_T n_{\text{PDC}} \left( \frac{-2\pi\mathbf{x}_T}{\lambda f} \right) \\ \times \left[ 1 + n_{\text{PDC}} \left( \frac{+2\pi\mathbf{x}_T}{\lambda f} \right) \right] \left[ 1 + n_{th} \left( \frac{-2\pi\mathbf{x}_T}{\lambda f} \right) \right]^2 \end{aligned} \quad (11)$$

As expected the correlation function in Eq. (11) reproduces the object transmission function and depends on the properties of our source through the mean photon numbers of the PDC and of the chaotic seeding field.

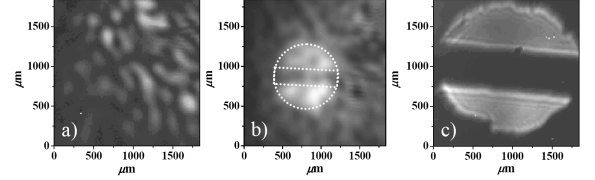


FIG. 3: a) Typical sample of chaotic single-shot Map  $I_R(\mathbf{x}_R)$  recorded on the Reference-arm; b) Image of the object recovered by evaluating  $G^{(2)}(\mathbf{x}_R)$  over 4000 laser shots; c) 1-to-1 image of the object illuminated by the beam in the Test arm (average over 500 laser shots). Note that the size of the image reconstructed in b) is one half that of the object image in c), in agreement with the value of the magnification,  $M = 0.5$ .

In Fig. 3 we show the experimental results: by calculating the averages in Eq. (6) over 4000 single shot Maps as the one in a) we obtained the  $G^{(2)}(\mathbf{x}_R)$  plotted in b), which shows a recovered image with the correct size, as compared to the object image in c), being  $M = 0.5$ . Note that the quality of the reconstructed image did not tremendously improve when the averages were calculated on a number of Maps,  $N$ , much greater than 4000.

In view of our application to a protocol of efficient encryption, it is interesting to establish a criterion for the choice of the minimum  $N$ , if it exists, that is needed for a satisfactory result. We define the local visibility [12]

$$\mathcal{V}(\mathbf{x}_R) = \frac{G^{(2)}(\mathbf{x}_R)}{\langle I_R(\mathbf{x}_R)I_T \rangle} = \frac{G^{(2)}(\mathbf{x}_R)}{\langle I_R(\mathbf{x}_R) \rangle \langle I_T \rangle + G^{(2)}(\mathbf{x}_R)} \quad (12)$$

and calculate it by averaging over different numbers of Maps. Figure 4 displays  $\mathcal{V}(\mathbf{x}_R)$  for  $N = 9500$  on a linear grey scale that covers the whole range from minimum ( $\mathcal{V} = 0.62 \times 10^{-3}$ ) to maximum ( $\mathcal{V} = 7.03 \times 10^{-3}$ ). The smaller panels show contour plots of the same  $\mathcal{V}(\mathbf{x}_R)$  at selected levels and the point at which  $\mathcal{V}(\mathbf{x}_{R,Max}) = 7.03 \times 10^{-3}$ .

The full dots of the upper curve in Fig. 5, in which the visibility is plotted as a function of  $N$ , show that already for  $N = 7000$  the visibility has roughly achieved such a value. Also in the four nearest neighbourhood of pixel  $\mathbf{x}_{R,Max} = (53, 32)$  we observe a similar behaviour (11) (see triangles with four orientations - up, down, left, and

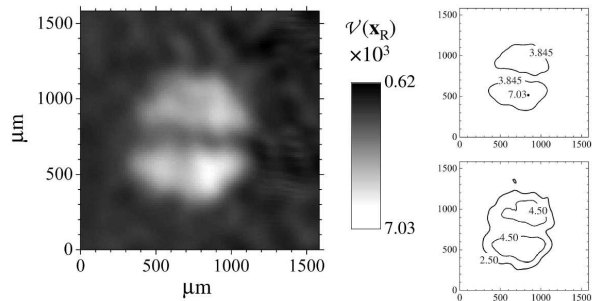


FIG. 4: Plot of the local visibility,  $\mathcal{V}(\mathbf{x}_R)$ , on a linear grey scale for  $N = 9500$  and of contours at the marked levels.

right - in the same curve). We further investigated the behaviour of  $\mathcal{V}(\mathbf{x}_R)$  on increasing  $N$  at a number of positions located next to the contours in Fig. 4. The positions on the three contours and their number for each contour were chosen by setting the tolerance values reported on the right-hand side of Fig. 5. We obtained the three sets of data that are plotted in Fig. 5 by increasing  $N$  in steps of 500. The figure shows that the values of  $\mathcal{V}(\mathbf{x}_R)$  calculated at positions virtually belonging to a level contour of the "best averaged" visibility map ( $N = 9500$ ) in all cases are similar to the final values for  $N \gtrsim 5000$ . Thus, not only the local visibility evaluated at the point,  $\mathbf{x}_{R,Max}$ , where it is maximum, but also that evaluated at any position is a measure of the ghost-image quality that can be obtained from a statistical ensemble of data of given size  $N$ .

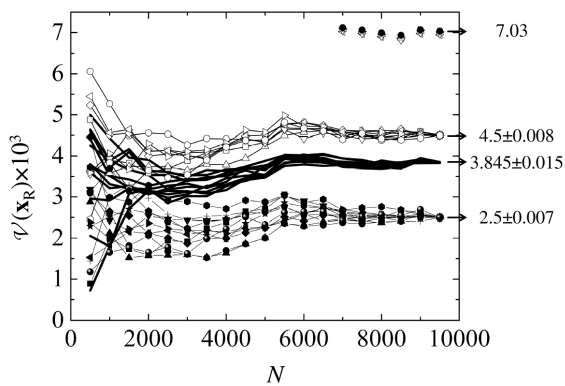


FIG. 5: Local visibility,  $\mathcal{V}(\mathbf{x}_R)$ , as a function of  $N$  calculated at points  $\mathbf{x}_R$  on the level contours of Fig. 4, see the values  $\mathcal{V}(\mathbf{x}_R) \pm$  tolerances for  $N = 9500$ .

We exploit the fact that it is not worthwhile to increase the value of  $N$  beyond a definite value, which is  $N \simeq 5000$  in our experiment, from the point of view of efficient encryption and image transmission and demonstrate that our encryption protocol is efficient for the number of chaotic Maps sufficient to reach a satisfactory visibility. Storing the information of an image of the object like that in Fig. 3 c) requires 89 Kbytes ( $114 \times 114$  matrix of 12-bit data), whereas storing the Code necessary to reconstruct the image by using 5000 Maps requires 44 Kbytes (5000 12-bit data). This means that by using our protocol, in which only the Code must be securely encrypted, we achieve a reduction of about 50% of the required quantum Key length. We performed a test in which we used a standard PC data compression program and obtained that the compressed file of the image reduced to 39 Kbytes. This size should be compared with the 44 Kbytes size of our Code file which, once compressed, reduces to 17 Kbytes, thus giving a reduction of about 40%.

Despite the fact that in the present case our scheme guarantees an effective reduction of the key consumption, we underline that this experiment does not prove that encryption of the Code is in any case advantageous with respect to the image itself. For this reason a deeper analysis is being carried out at our laboratories regarding resolution and the signal-to-noise ratio of the retrieved images obtainable with our setup, as well as the connection between these parameters and the size of the Code.

In conclusion, as QKD for secure image transfer is a difficult task, in order to reduce the key consumption we proposed a scheme for an efficient encryption of images that exploits distributed imaging techniques. The basic idea is the exploitation of a well known effect, ghost imaging, in a quite different context. We performed a rather new experiment of ghost imaging based on the correlations of the fields produced by a chaotically seeded PDC to produce a set of chaotic images and a Code, both necessary for reconstructing the image of the object. In a proof of principle we observed that the information storage of this Code resulted to be much smaller than that of the entire image. We suggest that, in situations that we quantitatively identify by using the visibility in Eq. (12), the Code can be more efficiently encrypted by any secure cryptographic Key and sent to the legitimate receiver, who will be able to reconstruct the image by using the decrypted Code together with the publicly announced chaotic images.

[1] N. Gisin, G. Ribordy, W. Tittel, and H. Zbinden, Rev. Mod. Phys. **74**, 145 (2002).

[2] "A Quantum Information Science and Technology roadmap. Part 2: Quantum cryptography" version 1.0,

- ARDA (2004), <http://qist.lanl.gov>.
- [3] A. Zeilinger, *Rev. Mod. Phys.* **71**, 288 (1996).
  - [4] T. Jennewein, C. Simon, G. Weihs, H. Weinfurter, and A. Zeilinger, *Phys. Rev. Lett.* **84**, 4729 (2000).
  - [5] R. J. Hughes, J. E. Nordholt, D. Derkacs, and C. G. Peterson, *New J. Phys.* **4**, 43, (2002).
  - [6] M. D'Angelo and Y. H. Shih, *Laser Phys. Lett.* **2**, 567 (2005) and references therein.
  - [7] E. Brambilla, A. Gatti, M. Bache, and L. A. Lugiato, *Phys. Rev. A* **69**, 023802 (2004).
  - [8] I. P. Degiovanni, E. Puddu, M. Bondani, and S. Castelletto, manuscript in preparation.
  - [9] A. Ferraro and M. G. A. Paris, *Phys. Rev A* **72**, 032312 (2005).
  - [10] A. F. Abouraddy, B. E. A. Saleh, A. V. Sergienko, and M. C. Teich, *J. Opt. Soc. Am.* **19** 1177 (2002).
  - [11] J. W. Goodman, *Fourier Optics* (McGraw-Hill, New York, 1968).
  - [12] A. Gatti, E. Brambilla, M. Bache, and L. A. Lugiato, *Phys. Rev. A* **70** (2004) 013802.